Journal of Alloys and Compounds 509 (2011) 7948–7952

Contents lists available at ScienceDirect

Journal of Alloys and Compounds

journal homepage: www.elsevier.com/locate/jallcom

Effects of growth temperature on structure and electrical properties of dielectric (Ba,Sr)TiO_3 capacitors with transparent conducting oxide electrodes

Yuan-Chang Liang*, Chiem-Lum Huang, Chia-Yen Hu

Institute of Materials Engineering, National Taiwan Ocean University, Keelung 20224, Taiwan

ARTICLE INFO

Article history:
Received 15 March 2011
Received in revised form 7 May 2011
Accepted 12 May 2011
Available online 19 May 2011

Keywords:
Characterization
Physical vapor deposition processes
Oxides

ABSTRACT

200 nm-thick BST thin films were grown on Zr-doped In_2O_3/$SrTiO_3$ (1 0 0) substrates at 550–750 °C. X-ray diffraction results show that the as-deposited BST films were polycrystalline with random crystallographic orientations. X-ray diffraction patterns reveal that the BST film grown at 650 °C had the best crystalline quality of all the deposition temperatures. Atomic force microscopy and secondary ion mass spectrometry showed that the surface and interface structures of the BST films became rough as the growth temperature increased. The BST film grown at 650 °C showed the best electrical properties, with a dielectric constant of 420 at 1 MHz, dielectric tunability of 32.1%, dielectric loss of 0.015 at 300 kV/cm, and a mean optical transmittance in visible wavelength of 71.3%.

© 2011 Elsevier B.V. All rights reserved.

1. Introduction

Perovskite barium strontium titanate $Ba_{1-x}Sr_xTiO_3$ (BST) has excellent dielectric properties. As a result, BST thin films have been used in tunable microwave devices, electro-optic switches, capacitor applications in dynamic random access memory, and decoupling capacitors integrated into monolithic circuits [1–3]. These applications rely strongly on the excellent structural and electrical performance of BST films. The process parameters for BST thin films have a profound influence on the physical properties of BST films [4,5]. The structural characteristics of BST films, such as their grain size and defects, affect their dielectric and tunable properties [6,7]. The type of bottom electrode also affects the crystalline quality, chemical homogeneity, and electrical performance of perovskite dielectric films [8,9].

Recently, there are several studies on fabricating transparent perovskite oxide devices based on transparent conducting glasses [10,11]. Moreover, combining an optically transparent single-crystal substrate with wide bandgap oxides to form thin-film transistors gives interesting opportunities for optical applications [12,13]. Previous studies report the electrical and optical properties of perovskite oxides on transparent single-crystal substrates [14,15]. Indium oxide, zinc oxide, and tin oxide are the most common optically transparent electronic conductors, and are widely used in optoelectronic devices [16,13]. However, transparent conducting oxides have different crystal structures and chemical constituents of than perovskite dielectric oxides. Hence, the most important issue in integrating perovskite dielectric oxides with transparent conducting oxides to form high-efficiency transparent devices is to understand the correlation between the microstructure and electrical properties of such heterostructures. This study reports the growth of Zr-doped In_2O_3 (ZIO) thin film on a transparent single-crystal $SrTiO_3$ (STO) (1 0 0) substrate as the bottom electrode. The resulting ZIO thin films possesed superior optoelectronic properties [17]. This study also examines the growth temperature dependence of the correlation between the microstructure and electrical properties of the BST thin films prepared by radio-frequency magnetron sputtering.

2. Experimental

210 nm-thick ZIO films were grown on the single-crystalline STO (1 0 0) substrates using radio-frequency magnetron sputtering in pure ambient argon at 500 °C. The target material was prepared on mixing the precursor oxide powders of ZrO_2 (5 wt%) and In_2O_3 (95 wt%), pressing the powders into a pellet, and sintering it to realize a high density. The Zr/In atomic ratio of the ZIO film is estimated to be 0.06 by X-ray photoelectron spectroscopy (XPS). The detailed binding states for the elements of ZIO thin films have been described elsewhere [17]. The ZIO film has a resistivity of $\sim 2.8 \times 10^{-4}\ \Omega$ cm. The 200 nm-thick $Ba_{0.6}Sr_{0.4}TiO_3$ thin films were following grown on ZIO-buffered STO substrates at various temperatures (550–750 °C). During the deposition of the BST thin films, the gas pressure of deposition was fixed at 30 mTorr with an Ar/O_2 ratio of 4:1.

The crystallographic structures of the films were analyzed with measurements of X-ray diffraction (XRD). The composition depth profiles of the films were examined using secondary ion mass spectrometry (SIMS). The surface morphology of the films was investigated with an atomic force microscope (AFM). The optical transmittance of the samples was measured using a UV–visible spectrometer.

Pt top electrodes were sputtered onto the surface of the BST thin films at room temperature for the measurements of electrical properties. The dielectric properties of BST thin films were measured at 1 MHz using an HP4284 impedance analyzer.

* Corresponding author.
E-mail addresses: yuanvictory@gmail.com, deanvera@yahoo.com.tw (Y.-C. Liang).

0925-8388/$ – see front matter © 2011 Elsevier B.V. All rights reserved.
doi:10.1016/j.jallcom.2011.05.046

The leakage current density was measured using an HP4140B pA meter/dc voltage source at room temperature.

3. Results and discussion

Fig. 1 shows the XRD pattern of the ZIO film grown on the single-crystalline STO (1 0 0) substrate. The Bragg reflections corresponding to ZIO (4 0 0) and (4 4 0) were observed in the XRD pattern, revealing a well crystalline ZIO film was formed on the STO substrate. Notably, the intensity of ZIO (4 0 0) Bragg reflection is quite weak in comparison with that of ZIO (4 4 0). The ZIO film on the STO (1 0 0) substrate shows a (4 4 0)-textured crystallographic structure. Moreover, the absence of Bragg reflections for ZrO_2 phase in the XRD pattern indicates the effective solid solution of Zr dopant in the In_2O_3 film.

Fig. 2 shows an AFM image of the ZIO/STO thin film prepared in this study. The surface morphology of this film clearly shows an orthogonal domain surface structure with a root-mean-square (rms) roughness of 5.53 nm. Previous studies report the crystallographic orientation-dependent morphology of surface grains for sputtered epitaxial ZIO and polycrystalline impurity-doped In_2O_3 films [18–20]. The (4 4 0)-textured crystallographic feature of the deposited film clearly results in the orthogonal domain surface structure of the polycrystalline ZIO film on the perovskite STO (1 0 0) substrate. This finding is consistent with previous research on sputtered polycrystalline Sn-doped In_2O_3 films [20].

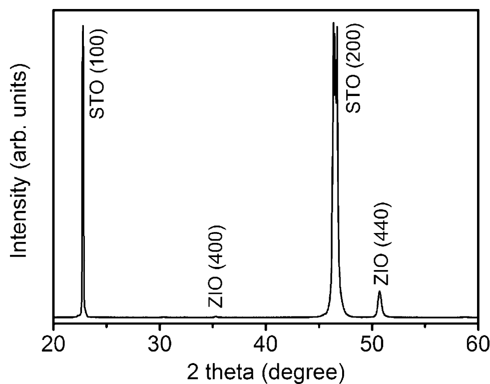

Fig. 1. XRD pattern of ZIO thin film on the STO (1 0 0) substrate.

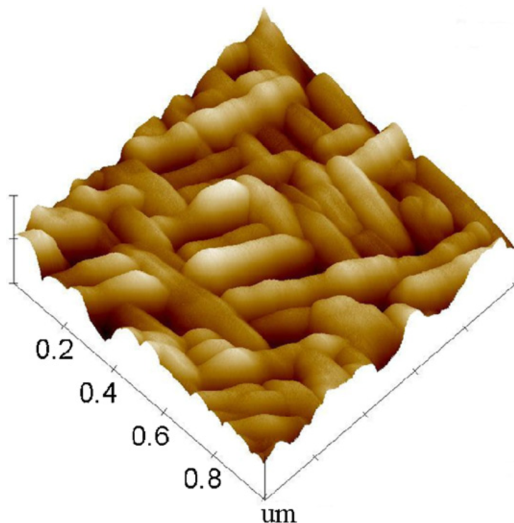

Fig. 2. AFM surface image of ZIO thin film grown on the STO (1 0 0) substrate.

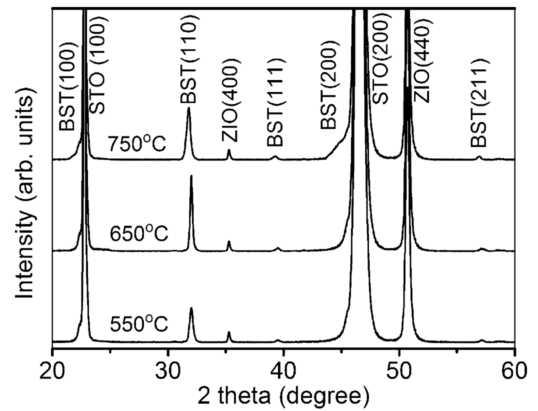

Fig. 3. XRD patterns of BST thin films grown on the ZIO/STO substrates at various temperatures.

Fig. 3 shows the XRD patterns of BST thin films grown on ZIO/STO substrates at various temperatures. These XRD patterns reveal Bragg peaks corresponding to the perovskite-structured BST phase. The as-deposited BST thin films showed a randomly oriented crystallographic feature. In this figure, the (1 1 0) orientation dominates the crystallographic feature in the polycrystalline BST thin films. Many researchers have shown a preference for the (1 1 0) orientation in BST films grown on substrates with crystal structure differ from that of the upper BST thin film layer [21]. The BST thin film grown at 550 °C had a higher full width at half maximum (FWHM) value and a lower (1 1 0) Bragg reflection intensity than the BST film grown at 650 °C. A higher growth temperature resulted in a higher crystalline quality of the film. However, as the growth temperature reached 750 °C, the FWHM value increased and (1 1 0) Bragg reflection intensity decreased. The BST thin film grown at 750 °C exhibited a clear shift in the Bragg peak to a relatively lower position compared to that grown at 650 °C. This might be attributed to more oxygen vacancies or defects in the BST thin film grown at a higher temperature [7]. Serious interdiffusion between the BST and ZIO thin films might occur at a growth temperature of 750 °C, which might also account for the worse crystalline quality of the high-temperature deposited BST thin film.

Fig. 4 shows the SIMS depth profiles of BST thin films grown on the ZIO-coated STO (1 0 0) substrates at various temperatures. The SIMS depth profiles of the BST thin film grown at 550 °C reveal a compositionally sharper interface with no obvious interdiffusion of constituent elements between the as-deposited dielectric BST film and the ZIO bottom electrode. The compositional profiles at the BST–ZIO interface became broader as the growth temperature increased. This may be because a high growth temperature

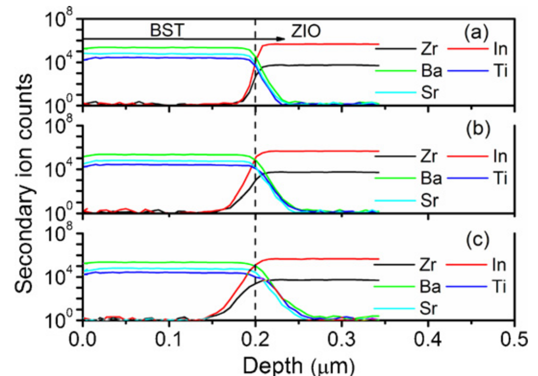

Fig. 4. SIMS depth profiles of BST/ZIO/STO films grown at various temperatures: (a) 550, (b) 650, and (c) 750 °C.

induced interdiffusion between the constituent oxide compounds. The existence of an interfacial layer due to the atomic interdiffusion of dielectric thin films grown on transparent conductive oxides degrades the electrical performance of perovskite dielectric films [10].

Fig. 5 shows the surface morphology of BST films grown at various temperatures on ZIO-coated STO substrates. The grain size of the BST film increased with growth temperature, creating a coarse surface. The rms roughness of BST films grown at 550, 650, and 750 °C was 3.19, 3.87, and 4.53 nm, respectively. The grain size increased with increasing growth temperature, creating a corresponding increase in surface roughness. Fig. 6 shows the optical transmittance of the BST/ZIO/STO films. The mean optical transmittance of STO substrate is around 81% [22]. The transparency of the BST films has been shown a clear drop in the UV region [23]. The absorption edges of the BST thin films are at the wavelength of ∼320 nm, which is close to that in literatures. The BST/ZIO/STO films grown at 550, 650, and 750 °C had mean optical transmittances of 74.5, 71.3, and 64.5%, respectively, in the visible wavelength regions. Changes in electronic structure due to crystal quality may be responsible for variations in the optical properties of BST thin films [24]. The rough film surface and many micro-defects in the BST film grown at 750 °C might be responsible for its serious decrease in optical quality. Optical transmittance data reveal that the BST films grown below 650 °C had satisfactory optical transparency over 70%.

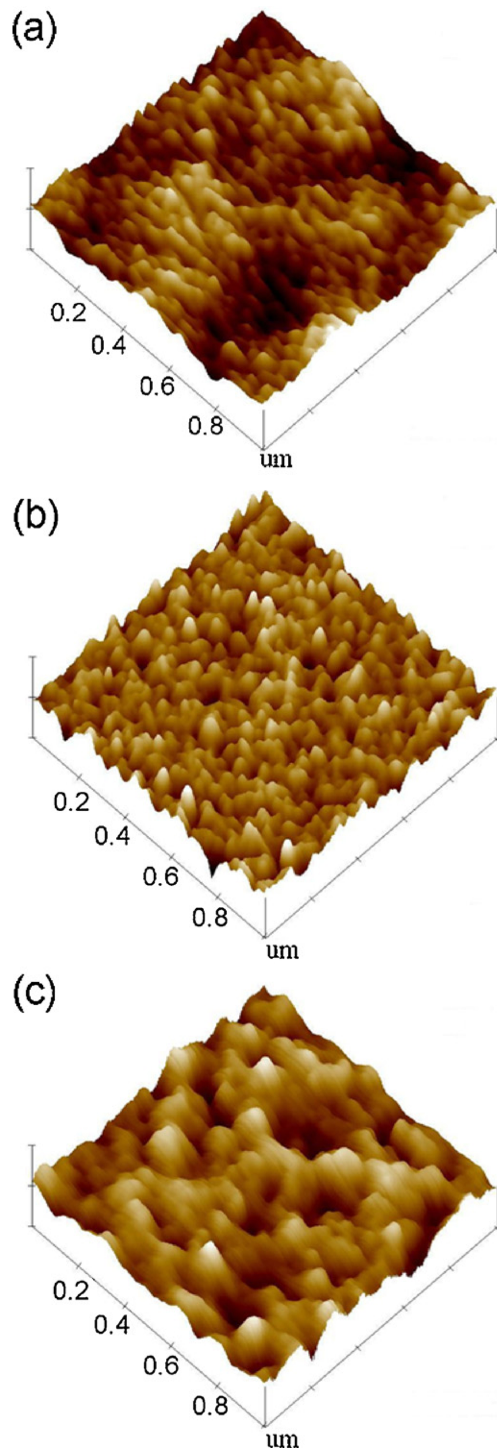

Fig. 5. AFM surface images of BST thin films grown on the ZIO/STO substrates at various temperatures.

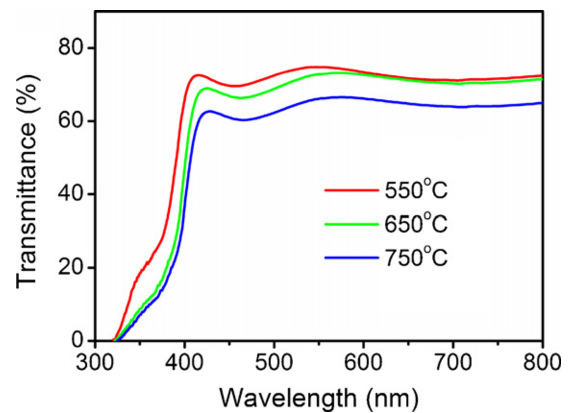

Fig. 6. Optical transmittance of BST/ZIO/STO films grown at various temperatures.

Fig. 7 shows the electrical properties of BST thin films grown on the ZIO/STO substrates at various temperatures. The BST thin films grown at 550, 650, and 750 °C had dielectric constants measured at 1 MHz of 372, 420, and 334, respectively. The BST film grown at 750 °C showed the worst dielectric constant. This might be due to the many defects in the film and serious interdiffusion between the BST dielectric layer and ZIO thin-film electrode. Fig. 7(a) shows the dielectric tunability of BST films as a function of applied electric field. This study defines dielectric tunability as $[\varepsilon(0)-\varepsilon(E)]/\varepsilon(0)$; where $\varepsilon(0)$ and $\varepsilon(E)$ are the dielectric constant at the zero electric field and applied electric field E, respectively [7]. The dielectric tunability at 300 kV/cm of the BST thin film grown at 550 °C was 22.4%, whereas that of the film grown at 650 °C reached 32.1%. The unsatisfactory dielectric tunability performance of the BST film grown at 550 °C was due to the poor crystallinity of the film. A further decrease in dielectric tunability in the BST films grown at 750 °C confirmed that a high growth temperature further deteriorates film quality. The BST film grown at 750 °C exhibited a low dielectric tunability of 13.5%. Fig. 7(b) shows the dielectric loss of BST films as a function of applied electric field. The BST film grown at 650 °C showed the lowest dielectric loss of 0.015 at 300 kV/cm, while those for BST films grown at 750 and 550 °C were 0.028 and 0.019 at 300 kV/cm, respectively. The BST film grown at 750 °C exhibited a large dispersion in the curve of dielectric loss vs. electric field. This could be associated with poor film homogeneity and the existence of an internal interfacial barrier [25]. The electrons resulting from the generation of oxygen vacancies forming during the high-temperature deposition of oxide thin films can hop between different titanium ions, inducing the reduction of Ti^{4+} to Ti^{3+}. This in turn provides a mechanism for dielectric losses [26]. A decrease in the number of grain boundaries increases conductivity. Thus, films deposited at a high temperature had higher dielectric loss

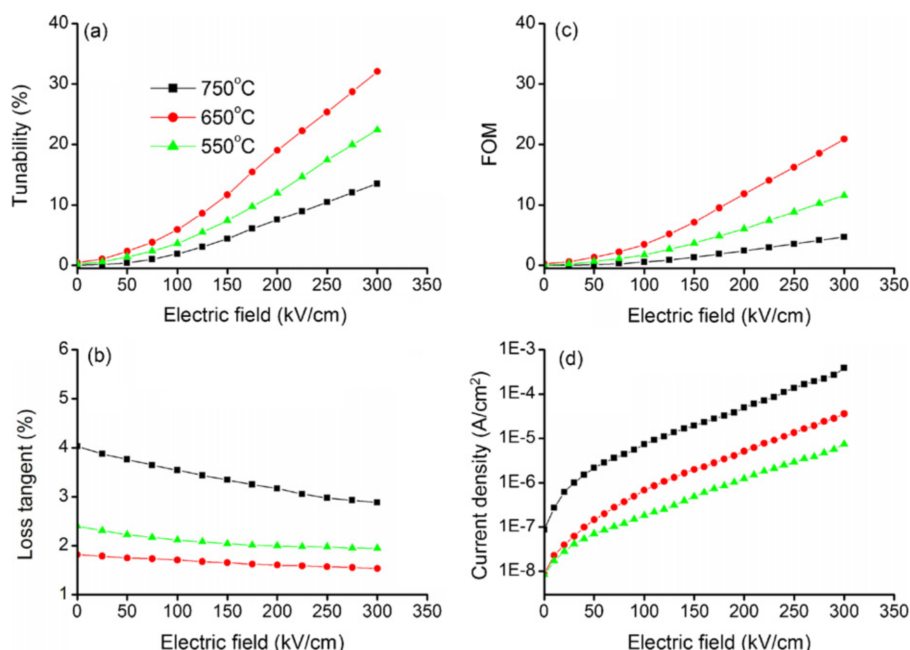

Fig. 7. Electrical properties of BST/ZIO/STO films grown at various temperatures: (a) tunability vs. electric field, (b) dielectric loss vs. electric field, (c) FOM values vs. electric field, and (d) current density vs. electric field.

due to contributions from resistive loss [27]. These factors explain why the BST film grown at 750 °C had a relatively large dielectric loss. Fig. 7(c) shows values of the figure of merit (FOM) for the BST films, where FOM is defined as tunability/dielectric loss. The FOM value measured at 300 kV/cm increased from 11.54 to 20.87 for BST films as the growth temperature increased from 550 to 650 °C. An increase in crystalline quality due to a higher growth temperature might account for this increase in the FOM value. However, a large decrease in the FOM value (from 20.87 to 4.68) occurred when the growth temperature of BST films increased from 650 to 750 °C, indicating that the film grown at 750 °C had an unsatisfactory FOM for tunable devices. Fig. 7(d) depicts the leakage current–voltage characteristics of BST films. In this figure, the BST film deposited at a relatively low temperature shows much better leakage current characteristics. A rougher surface and dielectric film interface structures may increase the leakage current [28]. Moreover, the grain size of BST film increased as the growth temperature increased. The grain boundary was the conduction path of the leakage current in the polycrystalline dielectric thin films. The BST film grown at 550 °C had smaller grains. These relatively small grains were more effective at blocking the short-cut routes in the film, and thus reduced the leakage current in the BST thin film deposited at a relatively low temperature [6,7].

4. Conclusions

The ZIO thin film grown on a STO substrate showed a (4 4 0)-textured crystallographic structure and an orthogonal domain surface structure. XRD patterns show that the BST thin film grown at 650 °C on this substrate had the best crystalline quality of all the samples. SIMS depth profiling showed that the BST and ZIO interface became rough as the growth temperature increased, which may be due to atomic interdiffusion at high temperatures. A high growth temperature resulted in a rougher surface structure, which further decreased the optical transmittance of the BST film. Electrical measurements demonstrated that the BST grown at 750 °C showed the worst dielectric and leakage current properties due to more defects, a rough surface, and interface film structures. However, the relatively low growth temperature of 550 °C produced BST films with lower crystalline quality, which also contributed to a deterioration in the electrical properties of the BST film on the ZIO/STO substrate. The BST film grown at 650 °C showed the best electrical properties, with a dielectric tunability of 32.1%, a dielectric loss of 0.015 at 300 kV/cm, and a mean optical transmittance of 71.3% in the visible wavelength regions.

Acknowledgements

This work is supported by the National Taiwan Ocean University (Grant No. NTOU-RD-AA-2010-104031) and the National Science Council of the Republic of China (Grant No. NSC 99-2221-E-019-055).

References

[1] T.J. Zhang, S.Z. Li, B.S. Zhang, R.K. Pan, W.H. Huang, J. Jiang, Ceram. Int. 33 (2007) 723.
[2] Y.C. Liang, Y.C. Liang, J. Electrochem. Soc. 154 (2007) G193.
[3] V. Reymond, D. Michau, S. Payan, M. Maglione, Ceram. Int. 30 (2004) 1085.
[4] F. Challali, M.P. Besland, D. Benzeggouta, C. Borderon, M.C. Hugon, S. Salimy, J.C. Saubat, A. Charpentier, D. Averty, A. Goullet, J.P. Landesman, Thin Solid Films 518 (2010) 4619.
[5] E.M. Kim, J.Y. Cho, J.H. Moon, W.J. Lee, H.S. Kim, J.H. Kim, Ceram. Int. 34 (2008) 1017.
[6] Y.C. Liang, Y.C. Liang, J.P. Chu, Electrochem. Solid State Lett. 11 (2008) G41.
[7] Y.C. Liang, J.P. Chu, Jpn. J. Appl. Phys. 47 (2008) 257.
[8] S. Ito, T. Yamada, K. Takahashi, S. Okamoto, T. Kamo, H. Funakubo, I. Koutsaroff, M. Zelner, A. Cervin-Lawry, J. Appl. Phys. 105 (2009) 061606.
[9] Y.C. Liang, Electrochem. Solid-State Lett. 12 (2009) G57.
[10] Y.C. Liang, Y.C. Liang, Scr. Mater. 61 (2009) 117.
[11] E. Bruno, M.P. De Santo, M. Castriota, S. Marino, G. Strangi, E. Cazzanelli, N. Scaramuzza, J. Appl. Phys. 103 (2008) 064103.
[12] M.W.J. Prins, K.O. Grosse-Holz, G. Muller, J.F.M. Cillessen, J.B. Giesbers, R.P. Weening, R.M. Wolf, Appl. Phys. Lett. 68 (1996) 3650.
[13] I. Titkov, I. Pronin, L. Delimova, I. Liniichuk, I. Grekhov, Thin Solid Films 515 (2007) 8748.
[14] Y.C. Liang, Thin Solid Films 518 (2010) S22.
[15] V. Fuflyigin, F. Wang, H. Jiang, J. Zhao, P. Norris, Appl. Phys. Lett. 76 (2000) 1641.
[16] Y.C. Liang, C.C. Liu, C.C. Kuo, Y.C. Liang, J. Cryst. Growth 310 (2008) 3741.
[17] Y.C. Liang, Y.C. Liang, Appl. Phys. A: Mater. Sci. Process. 97 (2009) 249.
[18] Y.C. Liang, H.Y. Lee, CrystEngComm 12 (2010) 3172.

[19] Y.C. Liang, Ceram. Int. 36 (2010) 1743.
[20] M. Kamei, Y. Shigesato, S. Takaki, Thin Solid Films 259 (1995) 38.
[21] B.T. Lee, C.S. Hwang, Appl. Phys. Lett. 77 (2000) 124.
[22] E. Bellingeri, I. Pallecchi, L. Pellegrino, G. Canu, M. Biasotti, M. Vignolo, A.S. Siri, D. Marré, Phys. Status Solidi A 205 (2008) 1934.
[23] D.Y. Wang, S. Li, H.L.W. Chan, C.L. Choy, Appl. Phys. Lett. 96 (2010) 061905.
[24] K.Y. Chan, W.S. Tsang, C.L. Mak, K.H. Wong, Phys. Rev. B 69 (2004) 144111.
[25] S.U. Adikary, H.L.W. Chan, Thin Solid Films 424 (2003) 70.
[26] M. Jain, S.B. Majumder, R.S. Katiyar, F.A. Miranda, F.W. Van Keuls, Appl. Phys. Lett. 82 (2003) 1911.
[27] M.S. Tsai, S.C. Sun, T.Y. Tseng, J. Appl. Phys. 82 (1997) 3482.
[28] Y.C. Liang, Y.C. Liang, Thin Solid Films 518 (2010) S17.